Journal of Radiation Research, Vol. 59, No. 4, 2018, pp. 501–510
doi: 10.1093/jrr/rry019
Advance Access Publication: 5 April 2018

Image quality improvement in cone-beam CT using the super-resolution technique

Asuka Oyama[1], Shinobu Kumagai[2], Norikazu Arai[2], Takeshi Takata[1], Yusuke Saikawa[1], Kenshiro Shiraishi[3], Takenori Kobayashi[1] and Jun'ichi Kotoku[1,2,*]

[1]Graduate School of Medical Care and Technology, Teikyo University, 2-11-1 Kaga, Itabashi-ku, Tokyo 173-8605, Japan
[2]Central Radiology Division, Teikyo University Hospital, 2-11-1 Kaga, Itabashi-ku, Tokyo 173-8606, Japan
[3]Department of Radiology, Teikyo University School of Medicine, 2-11-1 Kaga, Itabashi-ku, Tokyo 173-8605, Japan
*Corresponding author. Graduate School of Medical Care and Technology, Teikyo University, 2-11-1 Kaga, Itabashi-ku, 173-8605, Japan.
Email: kotoku@med.teikyo-u.ac.jp
(Received 20 June 2017; revised 28 August 2017; editorial decision 25 February 2018)

ABSTRACT

This study was conducted to improve cone-beam computed tomography (CBCT) image quality using the super-resolution technique, a method of inferring a high-resolution image from a low-resolution image. This technique is used with two matrices, so-called dictionaries, constructed respectively from high-resolution and low-resolution image bases. For this study, a CBCT image, as a low-resolution image, is represented as a linear combination of atoms, the image bases in the low-resolution dictionary. The corresponding super-resolution image was inferred by multiplying the coefficients and the high-resolution dictionary atoms extracted from planning CT images. To evaluate the proposed method, we computed the root mean square error (RMSE) and structural similarity (SSIM). The resulting RMSE and SSIM between the super-resolution images and the planning CT images were, respectively, as much as 0.81 and 1.29 times better than those obtained without using the super-resolution technique. We used super-resolution technique to improve the CBCT image quality.

Keywords: super-resolution; cone-beam CT; dictionary learning; sparse coding; deformable image registration

INTRODUCTION

Cone-beam computed tomography (CBCT), which can reveal much information related to internal organs and tissues, has been used increasingly in medical applications in recent years. For example, CBCT has been used in angiography CT, CT fluoroscopy, and 4D CT [1–4]. In particular, CBCT is extremely useful for radiation treatment. The application of CBCT to radiation treatment has been developed for the use of image-guided radiotherapy (IGRT), enabling high-accuracy radiotherapy [5, 6].

Recently, many approaches for the implementation of adaptive radiotherapy (ART), which allows real-time treatment adaptation based on the most recent patient anatomy, have been investigated for use in providing higher accuracy treatment. Although CBCT images provide the most up-to-date information for a human body, they are adversely affected by noise and artifacts, which degrade the image quality. The image quality is often so low that CBCT images cannot be used directly to compute the dose distribution for treatment planning.

A conventional method using low-quality CBCT images for ART transforms planning CT images to CBCT images using non-rigid functions. The method then uses these images for re-planning [7–9]. Nevertheless, it is difficult to ensure high positional accuracy using this method with soft tissues or flatus with particularly large positional displacement between two images.

Another method for improving CBCT images suppresses scatter or cupping artifacts. The dose distribution is computed directly from those improved images [10–12]. However, those methods are applicable only to images before reconstruction. Furthermore, a specific filter must be used to improve image quality.

As described herein, we propose an image-improving method using a super-resolution technique for upsampling a low-resolution image

(or noisy image) by combining it with a corresponding high-resolution image (or clean image) [13]. Two benefits are gained when applying this method to CBCT images. (i) No misregistration occurs between the CBCT image and the reconstructed image, which is useful for radiotherapy that requires high irradiation accuracy. (ii) This method can be adapted to the reconstructed image. Therefore, no special equipment or reconstruction technique is necessary in order to improve image quality.

An earlier study by Karimi *et al.* [14] examined reduction of the radiation dose by application of a super-resolution technique to CT images. Their method uses a few projections as low-resolution images and numerous projections as high-resolution images. Images reconstructed from a few projections were clarified using this technique. Most studies using super-resolution techniques have adopted this approach for image improvement for the same modality.

There are two fundamental differences between the study by Karimi *et al.* and our study. The specifications of the CBCT used for our study differ from the specifications of the CT used for the other study. The CBCT image quality is much lower than the CT image quality because of the effects of the scattered X-rays, which are greater for larger irradiated areas.

Another important difference is the purpose of using super-resolution. The method reported by Karimi *et al.* uses a few projections as low-resolution images and numerous projections as high-resolution images. Actually, the purpose of their study was to produce high-dose CT images from low-dose images by application of the super-resolution technique. By contrast, the purpose of the present study was to estimate high-quality CBCT images from other devices, and to use planning-CT images as high-resolution images.

We propose a method of improving CBCT image quality by application of the super-resolution technique using images taken from two modalities: planning CT and CBCT.

MATERIALS AND METHODS

Overview of the conventional super-resolution method

We start with a description of an overview of the conventional super-resolution method, which usually requires numerous high-resolution images. As a first step, the super-resolution method generates a matrix consisting of high-resolution image bases: 'atoms'. This matrix is called a high-resolution dictionary (D_H). The K-SVD [15] algorithm has been used to generate the dictionary. Then, the super-resolution method generates a low-resolution dictionary (D_L) from undersampling or by adding blur to high-resolution atoms in D_H. The D_L represents the low-resolution image atoms. A low-resolution image is represented as a linear combination of low-resolution atoms. Finally, the super-resolution image is inferred by replacing low-resolution atoms with high-resolution ones. Consequently, a high-resolution image is generated from a low-resolution one.

Overview of the proposed method

A schematic representation of our approach is presented in Fig. 1. As a first step, high-resolution images and low-resolution images must be acquired to construct dictionaries. For this study, the planning CT and CBCT images were regarded, respectively, as high-resolution and low-resolution images. As a second step, the dictionaries are created from those images. Then an input CBCT image is represented as a linear combination of the atoms in the low-resolution dictionary. Finally, the super-resolution image is inferred by replacing the atoms in the low-resolution dictionary with the atoms in the high-resolution dictionary. Details of this method are described in the following sections.

Database preparation

For this study, a set of full-pelvis-region images (planning CT and CBCT) of 30 patients with prostatic tumor was acquired using planning CT (Aquilion LB; Toshiba Medical Systems Corp.) and CBCT (On-Board Imager; Varian Medical Systems Inc.) after anonymization. The CBCT images were acquired 8.0 days (median; range, 7–37) after the planning CT image acquisition. They were resized down to 140 × 270 × 50 voxels to reduce the calculation time. Table 1 presents the imaging parameters.

We regarded CBCT images as low-resolution images and regarded planning CT images as high-resolution images. To generate a super-resolution database, planning CT images were registered to corresponding

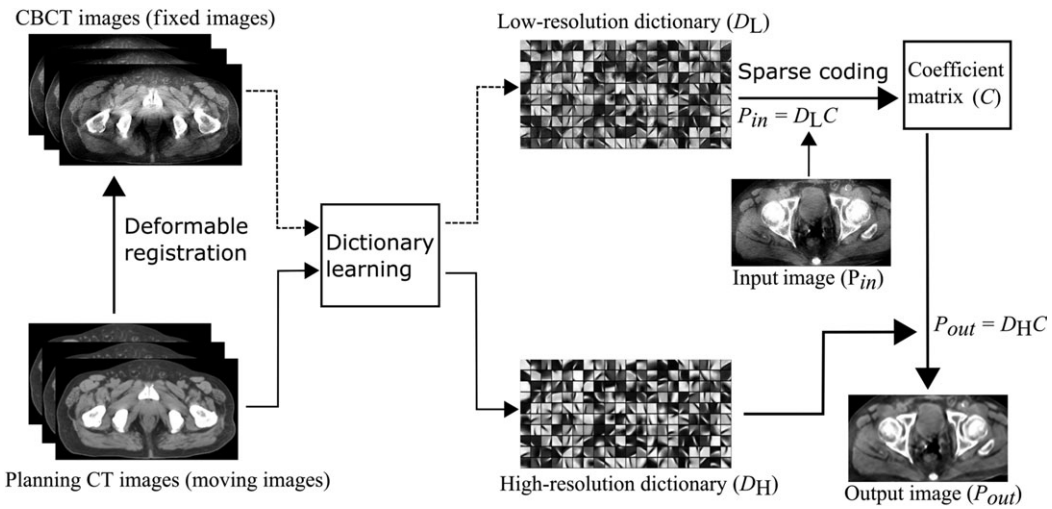

Fig. 1. Schematic representation of our proposed algorithm.

CBCT images using B-spline deformable registration. The resulting images are portrayed in Fig. 2. Then we extracted patches of size $\sqrt{n} \times \sqrt{n}$ from planning CT and CBCT images, where n denotes the number of elements in each patch. All patches were extracted with overlaps to increase the number of patches. Each element in the patch was represented as a vector ($\boldsymbol{p}^{\mathrm{H}} \in \mathbb{R}^n$ and $\boldsymbol{p}^{\mathrm{L}} \in \mathbb{R}^n$) and was arranged in a column of a matrix. Thus, we constructed the matrices $P_{\mathrm{H}} = [\boldsymbol{p}_1^{\mathrm{H}} \cdots \boldsymbol{p}_t^{\mathrm{H}}] \in \mathbb{R}^{n \times t}$ and $P_{\mathrm{L}} = [\boldsymbol{p}_1^{\mathrm{L}} \cdots \boldsymbol{p}_t^{\mathrm{L}}] \in \mathbb{R}^{n \times t}$, where t denotes the total number of patches within an image. We assumed that the k-th patches in these matrices (i.e., $\boldsymbol{p}_k^{\mathrm{H}}$ and $\boldsymbol{p}_k^{\mathrm{L}}$) are extracted from the same position of those images. By adapting this operation to all images, we generated a high-resolution database ($A_{\mathrm{H}} = [P_1^{\mathrm{H}} \cdots P_s^{\mathrm{H}}] \in \mathbb{R}^{n \times st}$) and a low-resolution one ($A_{\mathrm{L}} = [P_1^{\mathrm{L}} \cdots P_s^{\mathrm{L}}] \in \mathbb{R}^{n \times st}$), where s denotes the total number of images, and where P_k^{H} and P_k^{L} denote the matrix of the k-th image ($1 \leq k \leq s$). The high-resolution database A_{H} structure is presented in Fig. 3.

Construction of the low-resolution dictionary

This section presents a method for generating a dictionary from a prepared database A_{L}. We assumed that input signal $\boldsymbol{p}^{\mathrm{L}}$, which is extracted from an input image (low-resolution image), can be represented sparsely by $\boldsymbol{q} \in \mathbb{R}^m$ over the dictionary $D_{\mathrm{L}} \in \mathbb{R}^{n \times m}$, as

$$\boldsymbol{p}^{\mathrm{L}} = D_{\mathrm{L}} \boldsymbol{q} \tag{1}$$

where $\|\boldsymbol{q}\|_0 \ll n$. Here, $\|\cdot\|_0$ denotes the number of nonzero elements in the vector, called l_0-norm. In addition, $\boldsymbol{q}$ is a sparse coefficient vector representing the input signal's coordinates with fewer than n non-zeros.

For this study, we substituted a low-resolution database A_{L} for $\boldsymbol{p}^{\mathrm{L}}$ and substituted the matrix of combination coefficients $C \in \mathbb{R}^{m \times st}$ for $\boldsymbol{q}$ in the equation. A conceptual scheme of this equation is depicted in Fig. 4. The dictionary is learned under the constraint that the combination coefficient is sparse. This problem is presented by the following equation:

$$C^*, D_{\mathrm{L}}^* = \underset{C, D_{\mathrm{L}}}{\operatorname{argmin}} \|A_{\mathrm{L}} - D_{\mathrm{L}} C\|_2^2 \quad \text{subject to } \|C_i\|_0 \leq l. \tag{2}$$

Therein, C_i denotes the i-th column of C with only l or fewer non-zero coefficients. When the sparsity constraint is the l_0-norm as in Eq. (2), this optimization problem is classified as NP-hard [16]. Therefore, we relaxed Eq. (2) under the l_1-norm constraint to solve the problem as shown below.

$$C', D_{\mathrm{L}}{}^* = \underset{C, D_{\mathrm{L}}}{\operatorname{argmin}} \frac{1}{2}\|A_{\mathrm{L}} - D_{\mathrm{L}} C\|_2^2 + \lambda \|C\|_1 \quad \text{subject to } \|D_k^{\mathrm{L}}\|_2 = 1 \text{ for all } 0 \leq k < m_{\mathrm{atoms}}. \tag{3}$$

Here, m_{atoms} denotes the number of atoms in D_{L}, D_k^{L} represents the k-th column of D_{L}, and λ is a regularization parameter.

Then, we adopted functions of Mini-batch Dictionary Learning in scikit-learn (a machine learning library in Python) [17] to optimize Eq. (3) and to generate the low-resolution dictionary $D_{\mathrm{L}}{}^* \in \mathbb{R}^{n \times m}$. Here, regularization parameter λ is a fixed numerical value of 1.0. Inferred C' in Eq. (3) is no longer used in the following sections because it is a by-product in the construction of a low-resolution dictionary.

Table 1. Imaging parameters

	Planning CT	CBCT
Slice thickness [mm]	2.0	2.5
Pixel width [mm] range	0.877–1.074	0.651–1.172
X-ray tube voltage [kVp]	120	125
X-ray exposure [mAs] median (range)	250 (223–600)	682 (679–724)

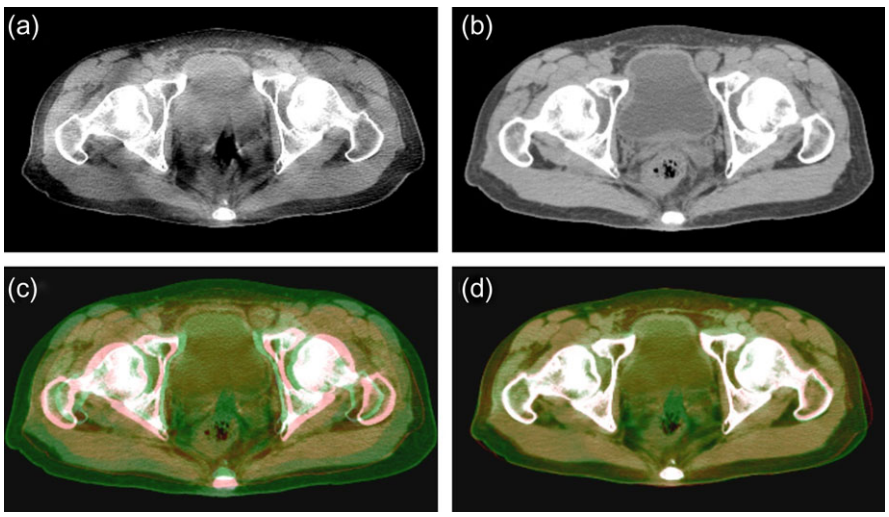

Fig. 2. Preparation images for database creation: CBCT image as a low-resolution image (a), planning CT image as a high-resolution image (b), alpha blending image of CBCT image (red) and planning CT image (green) before registration (c), and alpha blending image after registration (d).

Construction of the high-resolution dictionary

We solved the following equation and obtained coefficient matrix C^* of sparse representation C corresponding to database A_L. In this dictionary learning procedure, the orthogonal matching pursuit (OMP) [16] was used for sparse coding as

$$C^* = \mathrm{argmin}_C \|A_L - D_L^* C\|_2^2 \quad \text{subject to } \|C_i\|_0 \le l. \tag{4}$$

In that equation, C_i denotes the i-th column of C. This equation presented above is intended to solve the objective function in Eq. (3) as an l_0-norm minimization problem for the coefficient matrix. We can control sparsity (number of non-zero elements) by parameter l.

Finally, we constructed the high-resolution dictionary D_H [13]. We assumed that the high-resolution database A_H is reconstructed using a linear combination of atoms in D_H. Therefore, we sought dictionary D_H, which satisfies the following relation:

$$A_H \sim D_H C^*. \tag{5}$$

The solution of the problem in Eq. (5) is given as the following formula [13]:

$$D_H = A_H C^+ = A_H C^{*T} (C^* C^{*T})^{-1}. \tag{6}$$

Here, $\boldsymbol{C}^+$ represents a Moore–Penrose inverse matrix of $\boldsymbol{C}^*$. We generated $\boldsymbol{D_H}$ from Eq. (6). The resulting image of dictionary learning is presented in Fig. 5.

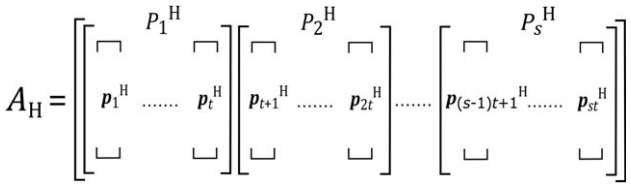

Fig. 3. Structure of high-resolution database $A_H \in \mathbb{R}^{n \times st}$: p_k^H denotes the vector of the extracted patch from the planning CT image $(1 \le k \le st)$; P_l^H denotes a matrix having p_k^H in each column $(1 \le l \le s)$; and A_H is the augmented matrix $(A_H = [P_1^H \cdots P_s^H])$.

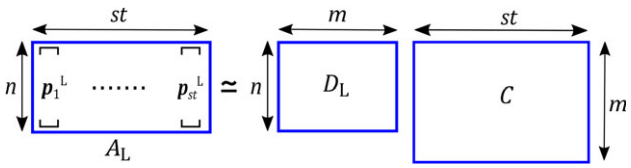

Fig. 4. Conceptual scheme showing relations between matrices: $A_L \in \mathbb{R}^{n \times st}$ is a low-resolution database; $D_L \in \mathbb{R}^{n \times m}$ is a low-resolution dictionary; and $C \in \mathbb{R}^{m \times st}$ is a combination coefficient.

Improved image estimation

Image reconstruction to improve the image quality of CBCT was done using the following steps.

(i) Extract patches from an input image in the manner described in 'Preparation of the database.' Each patch is arranged in a column $(\boldsymbol{p}_k^{in} \in \mathbb{R}^n, 1 \le k \le t)$. Here, n denotes the number of elements in a patch. t denotes the number of patches. Then, we obtained the set of patches $P_{in} = [\boldsymbol{p}_1^{in} \cdots \boldsymbol{p}_t^{in}] \in \mathbb{R}^{n \times t}$.

(ii) Apply the OMP algorithm on P_{in} and find a sparse representation matrix $C \in \mathbb{R}^{m \times t}$, in Fig. 6 and Fig. 7.

(iii) Multiply the matrix of combination coefficients C by high-resolution dictionary D_H, and infer a high-resolution set of patches using $P_{out} = D_H C \in \mathbb{R}^{n \times t}$.

(iv) Reconstruct the super-resolution image reconstructed from an input image by replacing the patches in P_{in} with the patches in P_{out} and by averaging the overlapped regions.

Quantitative evaluation

For the quantitative evaluation of registration accuracy, we computed normalized mutual information (NMI) and the Dice similarity coefficient (DSC) between the CBCT image and planning CT after registration. For similarity evaluation between images obtained from different modalities, NMI [18] is widely used. From two body contours (X and Y), which were extracted by threshold processing, DSC (i.e. $2[|X \cap Y|/(|X| + |Y|])$) was computed. The larger NMI and DSC signify that the two images are more similar. Furthermore, for quantitative evaluation of the output images, we computed the root

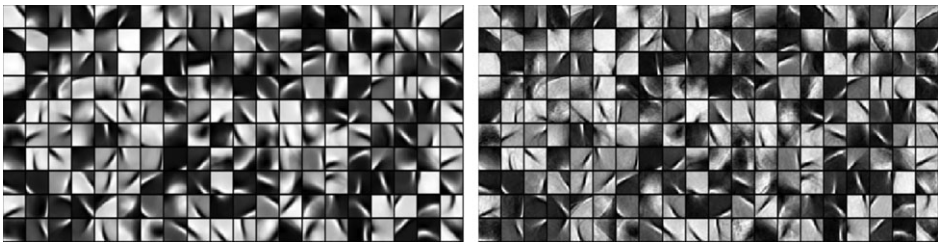

Fig. 5. Estimated high-resolution dictionary D_H (left) and low-resolution dictionary D_L (right). We present two sets of 200 chosen atoms from those dictionaries that have 400 atoms. Each atom is 20 × 20 pixels. Atoms of the same locations in all dictionaries mutually correspond.

mean square error (RMSE) and the structural similarity (SSIM) [19] between the images improved by super-resolution and the planning CT images.

Root mean square error

The RMSE is the standard deviation of the residuals between two images. Here, we designate a planning CT image as $X^P \in \mathbb{R}^{I\times J}$ and $X^{SR} \in \mathbb{R}^{I\times J}$ for a super-resolution image as

$$\mathrm{RMSE} = \sqrt{\frac{1}{n}\sum_{i=1}^{n}(X_i^P - X_i^{SR})^2}. \quad (7)$$

Here, n denotes the number of pixels. Also, X_i^P and X_i^{SR} denote the i-th pixels of those images. In general, a smaller RMSE reflects that fewer differences exist between two images.

Structural similarity

The SSIM is one method of evaluating the similarity between two images.

$$\mathrm{SSIM} = \frac{(2\mu_x\mu_y + \mathrm{K}_1)(2\sigma_{xy} + \mathrm{K}_2)}{(\mu_x^2 + \mu_y^2 + \mathrm{K}_1)(\sigma_x^2 + \sigma_y^2 + \mathrm{K}_2)}. \quad (8)$$

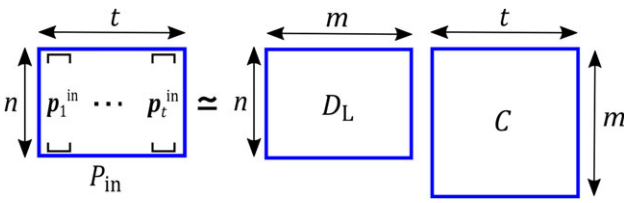

Fig. 6. Conceptual scheme showing relations among matrices: $P_{in} \in \mathbb{R}^{n\times t}$ is an input image; $D_L \in \mathbb{R}^{n\times m}$ is a low-resolution dictionary; and $C \in \mathbb{R}^{m\times t}$ is a combination coefficient.

Here, suffixes x and y, respectively, denote the super-resolution image and the planning CT image. The average of all pixel values is represented by μ, the standard deviation of the pixel values by σ, the covariance of two images by σ_{xy}, and fixed numbers by K_1 and K_2. In this study, a higher SSIM indicates higher similarity between a super-resolution image and a planning CT image.

Statistical analysis

For this study, Student's paired t test was used to assess differences between means in pixel values before and after reconstruction. Furthermore, Welch's t test was used to assess differences between mean in image Improvement and Non-improvement groups. All analyses were conducted using R ver. 4.3.2. Results for which $P < 0.05$ were inferred as significant.

RESULTS

Registration accuracy

The registration accuracy was computed between the CBCT image and planning CT after registration using NMI and DSC. The mean of NMIs was 0.231 (range 0.209–0.262). That of DSCs was 0.674 (range 0.546–0.794). Table 2 presents Welch's t test results for those evaluation indexes.

Optimization of parameters in dictionary learning

We demonstrated the application of our algorithm to whole-pelvis CT images of 30 patients. To obtain better results, we optimized the parameters in dictionary learning. One parameter is a patch size for extracting patches from images. During the optimization procedure, we attempted to set the patch sizes in the ranges of 5 × 5 to 50 × 50 pixels while maintaining all other parameters as fixed (Table 3). We evaluated the imaging quality using RMSE and SSIM. Figure 8 shows the improvement of image quality by comparison of those values. The optimum patch size is approximately 15 × 15 to 20 × 20 in Fig. 8. Refined images with a 20 × 20 patch size are presented in Fig. 9. These figures exhibit remarkable improvement in image quality in

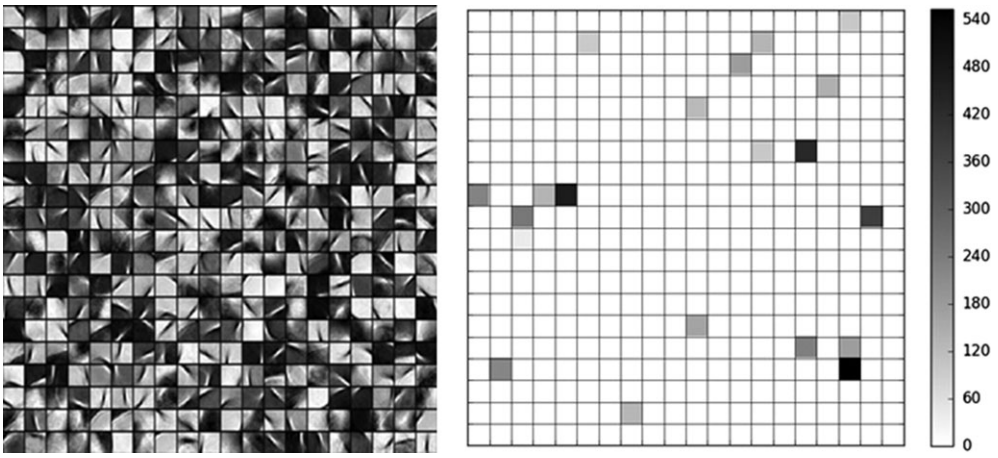

Fig. 7. Visualization of the combination coefficients obtained by orthogonal matching pursuit by atoms = 400 and $l = 20$. Mapping of the combination coefficients multiplied by the corresponding atoms in D_L (left) is shown (right): mapped zero coefficients are white; non-zero coefficients are gray.

Table 2. Assessment of differences between NMI and DSC means in images Improvement and Non-improvement groups using Welch's *t* test

	n	NMI			DSC		
		Mean (min–max)	*P* value	95% CI	Mean (min–max)	*P* value	95% CI
I	27	0.232 (0.21–0.26)	0.10	(−0.04, 0.03)	0.675 (0.55–0.79)	0.79	(−0.12, 0.15)
U	3	0.220 (0.22–0.23)			0.664 (0.59–0.70)		

CI = confidence interval, I = Improvement group, U = Non-improvement group.

Table 3. Fixed parameters of dictionary learning

Parameters	Values
Number of slices *s*	50
Number of atoms *m*	400
Regularization parameter λ	1.0
Iteration	5000

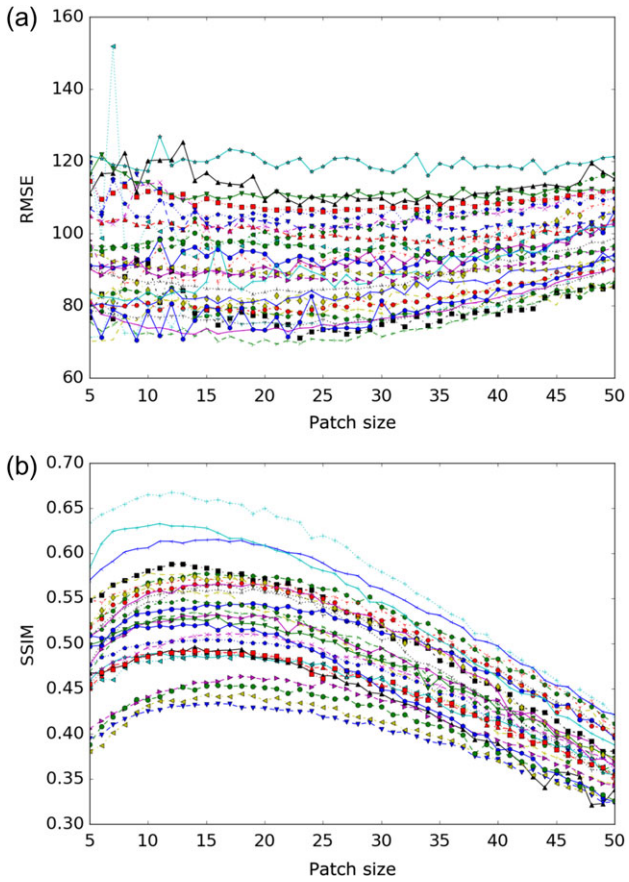

Fig. 8. Quantitative evaluation comparison for 30 patients. Patch sizes range from 5 × 5 to 50 × 50. Shown are the root mean square error (RMSE) (a) and the structural similarity (SSIM) (b).

terms of suppression of cupping artifacts and enhancement of the organ boundaries.

Quantitative evaluation result

Results of the quantitative evaluation of the proposed method showed that the values of RMSE between the original CBCT images and the planning CT images at bladder and prostate levels were 72.51–186.55 (minimum–maximum value) for all patients. The values of SSIM were 0.31–0.59. The values of RMSE between the reconstructed images and the planning CT images were 63.79–158.72. Additionally, the values of SSIM were 0.37–0.64. From the quantitative evaluation results, 56 regions out of 60 (two regions per patient) show image quality improvement. Of 30 patients, 27 showed improved image quality in both regions. Those results demonstrate that the values of RMSE and the SSIM were 0.81 and 1.29 times at the maximum (0.90 and 1.13 times at the mean) better than those original CBCT images, respectively. Furthermore, assessment of differences between means before and after reconstruction using Student's paired *t* test and 95% confidence intervals (CIs) revealed that the quality of each reconstructed image was improved significantly (Table 4). Figure 10 and Fig. 11, respectively, present quantitative comparisons of pelvis CT images.

Moreover, assessment of differences between two groups (with improvement and without improvement) using Welch's *t* test and 95% CIs revealed that the evaluation indexes of original CBCT images in the Non-improvement group showed better values than those of the Improvement group (Table 5).

DISCUSSION

Artifacts affected CBCT images, thereby reducing their image quality considerably. This paper presents a method for suppression of these artifacts using a super-resolution technique, thereby improving the CBCT image quality. The results of RMSE and SSIM in the super-resolution images were, respectively, as much as 0.81 times and 1.29 times better than those obtained from the planning CT images without the super-resolution technique. In addition, our method achieved high positional accuracy by including the latest internal body information at the time of CBCT imaging.

The results of the visual and quantitative evaluation (RMSE and SSIM) confirmed the image quality improvement. However, in some cases, the image quality was not improved greatly by quantitative evaluation. A possible reason is that those cases have low registration accuracy in the dictionary learning section. From Welch's *t* test results, we were unable to find a significant difference between NMI/DSC in the Improvement and Non-improvement groups (Table 2). For three

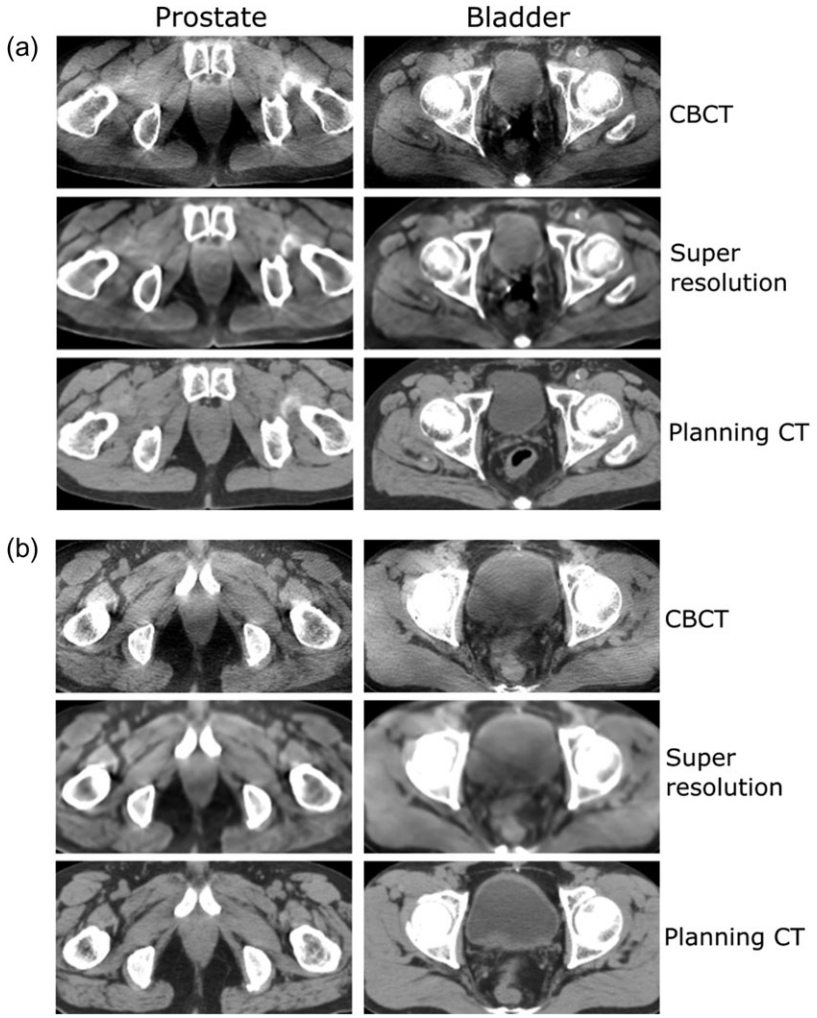

Fig. 9. Example images of application to pelvis CT images (a). Images of prostate level (left column). Images of bladder level (right column). CBCT images before processing (top row). Processed super-resolution images (middle row). Planning CT images with the same slice as the CBCT image (bottom row). The worst result of quantitative evaluation (b).

Table 4. Assessment of differences between means in images before and after reconstruction using Student's paired *t* test (bladder, *n* = 30; prostate, *n* = 30)

		n	RMSE			SSIM		
			Mean (min–max)	*P* value	95% CI	Mean (min–max)	*P* value	95% CI
B	BR	30	95.4 (72.5–186.5)	0.15	(−2.89, 17.98)	0.46 (0.31–0.57)	<0.01	(−0.08, 0.02)
	AR	30	87.9 (63.8–158.7)			0.51 (0.37–0.59)		
P	BR	30	100.8 (75.3–137.5)	<0.01	(4.38, 18.46)	0.46 (0.35–0.59)	<0.001	(−0.10, −0.04)
	AR	30	89.3 (69.8–121.4)			0.53 (0.43–0.64)		

CI = confidence interval, B = bladder, P = prostate, BR = before registration images, AR = after registration images.

patients in the Non-improvement group, however, NMI were 0.229, 0.216 and 0.215, and DSC were 0.704, 0.695 and 0.592. The NMIs in the Non-improvement group were lower than the mean NMI (0.231). Moreover, the DSC of one case was lower than the mean of DSC (0.674). Therefore, we infer that the registration error influenced those results.

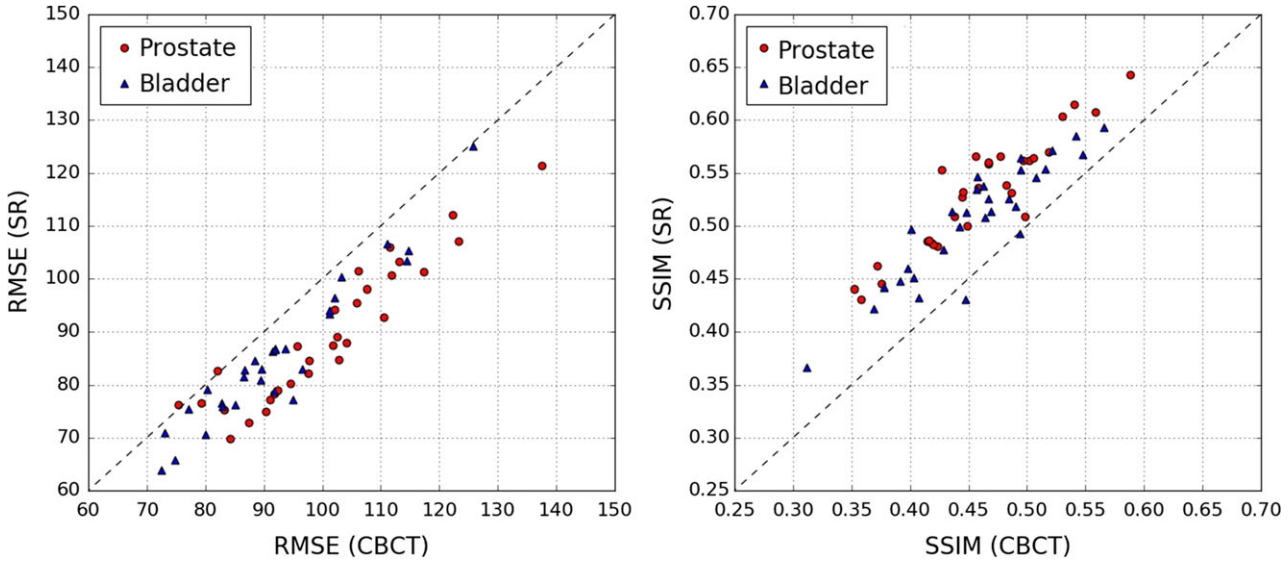

Fig. 10. Quantitative comparison of qualities of pelvis CT images with scatter plots of root mean square error (RMSE) (left) and structural similarity (SSIM) (right) for 30 patients. Image quality was evaluated at the prostate and bladder. Markers show that RMSE and SSIM were improved by application of the proposed method to images. CBCT = cone beam CT image, SR = super-resolution image.

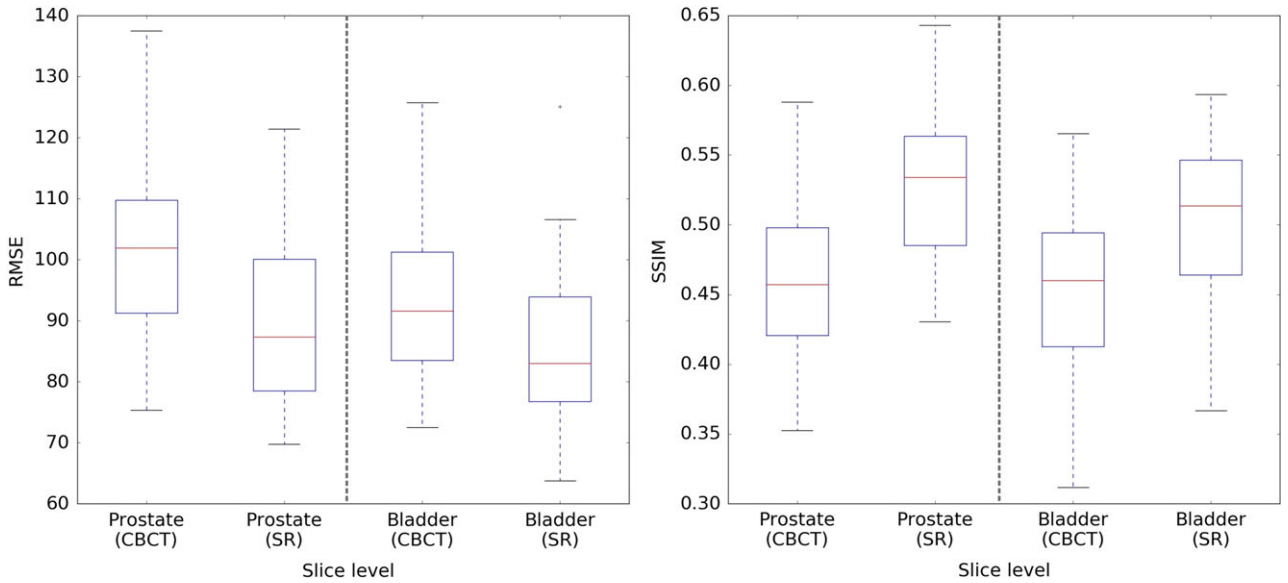

Fig. 11. Root mean square error (RMSE) (left) and structural similarity (SSIM) (right) for 30 patients: pelvis CT images at different slice levels.

Another possible reason is that the original CBCT images before application of the super-resolution method closely resembled the planning CT images, meaning that the original CBCT images were not degraded to any great degree in comparison with the planning CT images. Table 5 shows that the Non-improvement group has smaller RMSEs and higher SSIM values than those of the Improvement group. Therefore, the original CBCT images in the Non-improvement group were similar to the planning CT images. Such image quality was not improved with respect to the quantitative evaluation. Nonetheless, as presented in Fig. 9b, the results showed suppression of the cupping artifacts and enhancement of the organ boundaries.

The proposed method based on the super-resolution technique achieved higher positional accuracy than a conventional method using a non-rigid function [7–9]. As shown in Fig. 12, it is noteworthy that our method was able to include the latest internal body information at the time of CBCT imaging, e.g. indicating position changes due to

Table 5. Assessment of differences between means in images of the Improvement and Non-improvement groups using Welch's *t* test

		n	RMSE			SSIM		
			Mean (min–max)	*P* value	95% CI	Mean (min–max)	*P* value	95% CI
B	I	28	96.2 (72.5–186.5)	0.32	(−31.24, 54.44)	0.46 (0.31–0.57)	0.53	(−0.17, 0.13)
	U	2	84.6 (77.2–92.0)			0.47 (0.45–0.49)		
P	I	28	102.3 (79.3–137.5)	<0.05	(7.95, 39.25)	0.46 (0.35–0.59)	<0.05	(−0.08, −0.03)
	U	2	78.7 (75.3–82.1)			0.51 (0.51–0.52)		

CI = confidence interval, B = bladder, P = prostate, I = Improvement group, U = Non-improvement group.

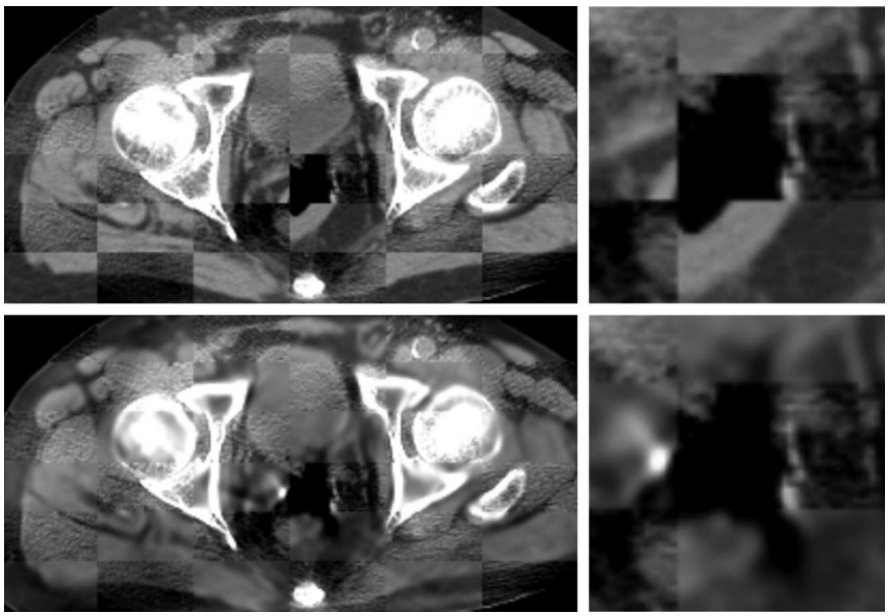

Fig. 12. Checkerboard images: upper left, a checkerboard of the CBCT image and planning CT image after registration; lower left, a checkerboard of the CBCT image and output image; right, an enlarged view of the part flatus in the left images.

flatus or organ movement of the patient. Therefore, this method can play an important role in radiation therapy that requires highly accurate irradiation.

Although we demonstrated the capabilities of our method using whole-pelvis CT images in this study, our method is not restricted to pelvic images. The quality of CBCT images taken from areas of the body other than the pelvis is also expected to be improved using dictionaries constructed from their CBCT images and planning CT images.

Several candidates for improving image quality exist. One approach is to increase the number of images for dictionary composition. For this study, we used a set of patient images per dictionary. The set included 50 images, providing a set of 1 287 750 patch-pairs. In general, the image quality becomes higher when using more data for dictionary learning [13]. If more images are used for learning, then it will be possible to construct a dictionary that can provide higher accuracy. In addition, the reconstructed image quality will be improved by increasing the number of atoms in the dictionary, which would also require increased computation time for the reconstruction [14].

Another approach is to acquire better registration accuracy. The conventional super-resolution method does not rely on the assumption that misregistration exists between image pairs used for dictionary learning. Therefore, misregistration might engender erroneous correspondence of atoms and might influence the reconstructed image quality. For this study, planning CT images were registered to corresponding CBCT images using B-spline deformable registration, but a limit was imposed to ensure high positional accuracy in soft tissues or flatus, as shown in Fig. 2. Even though registration was not perfect, our method showed a marked improvement in CBCT image quality, as shown in Fig. 9. Better registration accuracy will engender better performance of the algorithm.

Our study revealed that the super-resolution technique improves CBCT images from the corresponding planning CT images. This study specifically examined a CBCT image quality improvement technique. The proposed method is applicable not only to parts of the body other than the pelvis, but also to images obtained using other modalities.

CONFLICT OF INTEREST

The authors declare that there are no conflicts of interest.

FUNDING

This work was supported in part by the Japan Society for the Promotion of Science KAKENHI [Grant No. 15K08703].

REFERENCES

1. Jin J-Y, Ren L, Liu Q et al. Combining scatter reduction and correction to improve image quality in cone-beam computed tomography (CBCT). *Med Phys* 2010;37:5634–44.
2. Sun Z, Aziz YFA, Ng KH. Coronary CT angiography: how should physicians use it wisely and when do physicians request it appropriately? *Eur J Radiol* 2012;81:e684–7.
3. Murphy K, Nussbaum DA, Gailloud P. CT fluoroscopy: novel application for the treatment of ventricular pathologies. *Neuroradiology* 2007;49:373–8.
4. Li Y, Ma J, Chen X et al. 4DCT and CBCT based PTV margin in stereotactic body radiotherapy (SBRT) of non-small cell lung tumor adhered to chest wall or diaphragm. *Radiat Oncol* 2016;11:152.
5. Wang X, Li J, Wang P et al. Image guided radiation therapy boost in combination with high-dose-rate intracavitary brachytherapy for the treatment of cervical cancer. *Brachytherapy* 2016;8:122–7.
6. Jaffray DA, Siewerdsen JH, Wong JW et al. Flat-panel cone-beam computed tomography for image-guided radiation therapy. *Int J Radiat Oncol Biol Phys* 2002;53:1337–49.
7. Kurz C, Kamp F, Park Y-K et al. Investigating deformable image registration and scatter correction for CBCT-based dose calculation in adaptive IMPT. *Med Phys* 2016;43:5635–46.
8. Paquin D, Levy D, Xing L. Multiscale registration of planning CT and daily cone beam CT images for adaptive radiation therapy. *Med Phys* 2009;36:4–11.
9. Park SB, Rhee FC, Monroe JI et al. Spatially weighted mutual information image registration for image guided radiation therapy. *Med Phys* 2010;37:4590–601.
10. Niu T, Sun M, Star-Lack J et al. Shading correction for on-board cone-beam CT in radiation therapy using planning MDCT images. *Med Phys* 2010;37:5395–406.
11. Ning R, Tang X, Conover D. X-ray scatter correction algorithm for cone beam CT imaging. *Med Phys* 2004;36:1195–202.
12. Chen Y, Song Y, Ma J et al. Optimization-based scatter estimation using primary modulation for computed tomography. *Med Phys* 2016;43:4753–67.
13. Elad M. *Sparse and Redundant Representations: From Theory to Applications in Signal and Image Processing*. New York: Springer-Verlag, 2010.
14. Karimi D, Ward R. Reducing streak artifacts in computed tomography via sparse representation in coupled dictionaries. *Med Phys* 2016;43:1473–86.
15. Aharon M, Elad M, Bruckstein A. K-SVD: an algorithm for designing overcomplete dictionaries for sparse representation. *IEEE Trans Signal Process* 2006;54:4311–22.
16. Irina R, Genady Y. *Sparse Modeling: Theory, Algorithms, and Applications*. Boca Raton: CRC Press, 2014.
17. Mairal J, Bach F, Ponce J et al. Online dictionary learning for sparse coding. *Proc 26th Int Conf Mach Learn* 2009:1–8.
18. Strehl A, Ghosh J. Cluster ensembles—a knowledge reuse framework for combining multiple partitions. *J Mach Learn Res* 2002;3:583–617.
19. Wang Z, Bovik AC, Sheikh HR et al. Image quality assessment: from error visibility to structural similarity. *IEEE Trans Image Process* 2004;13:600–12.